Transition Met Chem (2014) 39:831–841
DOI 10.1007/s11243-014-9865-2

Spectroscopic characterization of chloride and pseudohalide ruthenium(II) complexes with 4-(4-nitrobenzyl)pyridine

Anna M. Maroń · Jan G. Małecki

Received: 29 May 2014 / Accepted: 28 July 2014 / Published online: 17 August 2014

Abstract Chloride, isocyanate and isothiocyanate hydride carbonyl ruthenium(II) complexes of 4-(4-nitrobenzyl)pyridine were synthesized from the precursor complex [RuHCl(CO)(PPh_3)$_3$] and characterized by IR, NMR, UV–Vis spectroscopy and X-ray crystallography. The electronic structures of the complexes were investigated by means of DFT calculations, based on their crystal structures. The spin-allowed singlet–singlet electronic transitions of the complexes were calculated by time-dependent DFT, and the UV–Vis spectra are discussed on this basis. The emission properties of the complexes were studied at ambient temperature, and the quantum yields of fluorescence, the lifetimes and nature of the excited states are discussed. The chloride and isothiocyanate complexes are practically nonemissive, with quantum yields under 0.01 %. Interpretation of spectra, supported by TD-DFT calculations, indicates that in this energy region, the transitions have MLCT character with admixture of LLCT (chloride and isothiocyanate complexes). The dominant LLCT character was visible in the case of the most emissive (isocyanate) complex. The low values of the lifetimes and quantum yields for these complexes indicate the influence of the metal center in the emission process.

Electronic supplementary material The online version of this article (doi:10.1007/s11243-014-9865-2) contains supplementary material, which is available to authorized users.

A. M. Maroń (✉) · J. G. Małecki
Department of Crystallography, Institute of Chemistry, University of Silesia, ul. Szkolna 9, 40-006 Katowice, Poland
e-mail: ank806@wp.pl

Introduction

Luminescent ruthenium(II) complexes are of interest of due to their applications in photochemical molecular devices (PMD) such as OLED devices, dye-sensitized solar cells (DSSC), photosensitizers in artificial photosynthesis, sensors, DNA dynamic probes, lipid probes and fluorescence polarization immunoassays (FPI) [1–11]. Recent descriptions of the photochemistry of coordination compounds of ruthenium(II) indicate that they can fulfill many of the functions necessary for these devices [1]. One of the most studied classes of ruthenium(II) complexes are polypyridine complexes [11–15]. In these species, strong emission in ambient temperature solutions is attributed to ^{3}MLCT states, but the photophysics and photochemistry of cationic polypyridine complexes depend also on the accessibility of short lived ($\tau = 5 - 20$ ns or less) ^{3}MC states [1]. However, the coordination environments of this metal based on the precursor complex [RuHCl(CO)(PPh_3)$_3$] have been little described with respect to their photophysical and photochemical properties. Phosphine complexes of ruthenium(II) based on [RuHCl(CO)(PPh_3)$_3$] have recently been studied as effective and selective catalysts in organic synthesis, but are much less known as luminophores.

It is well know that the spectroscopic properties of ruthenium(II) complexes can be tuned by the introduction of appropriate ligands. On the one hand, *N*-heterocyclic π-acceptor ligands determine the character of the unoccupied LUMO orbital. On the other hand, it is known that pseudohalide ligands tune the t_{2g} ruthenium orbitals by distributing the $4d_{Ru}$ energy levels over a wide energy range, due to mixing with orbitals centered on the thiocyanate (NCS) ligand [15–17]. Thus, studies of the electronic structures of these complexes are an important area of chemistry. In our recent studies on hydride carbonyl

complexes with *N*,*O*-donor ligands, we also observed the influences of triphenylphosphine and carbonyl ligands on their fluorescent properties [18, 19].

In this work, we present the synthesis, and characterization of ruthenium(II) hydride-carbonyl chloride, cyanate and isothiocyanate complexes with 4-(4-nitrobenzyl)-pyridine as co-ligand. It is known that free 4-(4-nitrobenzyl)-pyridine itself is nonemissive, but coordination leads to complexes with LUMOs dominated by π^* orbitals of the pyridine derivative. The character of the excited states of the complexes depends mostly on effects of the halide (Cl^-) or pseudohalide (SCN^-, NCO^-) ligands on the HOMO. Characterization of the complexes by X-ray crystallography and IR, NMR, and absorption and emission UV–Vis spectroscopy are complemented by theoretical calculations with the use of DFT. The quantum chemical study included the characterization of the molecular and electronic structures of the complexes by analysis of optimized molecular geometries. Finally, time-dependent density functional theory (TD-DFT) was used to calculate the electronic absorption spectra. Based on a molecular orbital scheme, these results allowed for the interpretation of the experimental UV–Vis spectra. The fluorescence properties (spectra, quantum yields, lifetime) are used to characterize the excited states.

Experimental

All reagents used for the syntheses were commercially available and used without further purification. The starting complex $[RuHCl(CO)(PPh_3)_3]$ was synthesized according to the literature method [20].

Synthesis of the complexes

These complexes were synthesized by the reaction of $[RuHCl(CO)(PPh_3)_3]$ (0.2 g, 2×10^{-4} mol), 4-(4-nitrobenzyl)pyridine (0.047 g, 2.2×10^{-4} mol) (**1**), sodium cyanate (0.016 g, 2.2×10^{-4} mol) (**2**), or ammonium thiocyanate (0.014 g, 2.2×10^{-4} mol) (**3**) in methanol (100 mL). The reaction mixture was refluxed for 6 h. After this time, it was cooled and filtered. Crystals suitable for X-ray crystal analysis were obtained by slow evaporation of the reaction mixtures.

*$[RuHCl(CO)(PPh_3)_2(NO_2PhCH_2py)]$ (**1**)*

Yield 58 %. $C_{49}H_{41}ClN_2P_2Ru$. Anal. calc: C 68.7 H 4.8 N 3.3 %. Anal. found: C 68.7 H 4.9 N 3.3 %. IR (KBr; cm^{-1}): 3,053 $\nu_{(ArH)}$; 2,051, 2,017 $\nu_{(Ru–H)}$; 1,919 $\nu_{(CO)}$; 1,594 $\nu_{(asym\ NO2)}$; 1,480 $\delta_{(C–CH\ out\ of\ the\ plane)}$; 1,432 $\nu_{Ph(P–Ph)}$; 1,343 $\nu_{(sym\ NO2)}$; 1,091 $\delta_{(C–CH\ in\ the\ plane)}$; 743 $\delta_{(C–C\ out\ of\ the\ plane)}$; 693 $\delta_{(C–C\ in\ the\ plane)}$; 518 $\nu_{(N;P–Ru)}$. ^{1}H NMR (500 MHz, $CDCl_3$) δ 8.30–8.12 (m, pybenzylNO$_2$), 7.85–7.36 (m, pybenzylNO$_2$), 7.36–7.12 (m, PPh$_3$/pybenzylNO$_2$), 4.06 (s, CH_2 from pybenzylNO$_2$), −13.50 (*t*, $J = 19.6$ Hz, $H_{(Ru)}$). ^{31}P NMR (202 MHz, $CDCl_3$) δ 45.57 (d, $J = 6.4$ Hz, PPh_3). ^{13}C NMR (126 MHz, $CDCl_3$) δ 204.18 (s), 153.90 (s), 152.47 (d, $J = 7.3$ Hz), 149.79 (s), 149.55 (s), 147.08 (d, $J = 4.5$ Hz), 145.52 (s), 145.32 (s), 136.43–133.77 (m), 133.55 (d, $J = 9.8$ Hz), 132.98 (s), 132.67–131.93 (m), 129.88 (s), 129.34 (s), 128.52 (d, $J = 12.1$ Hz), 128.15 (s), 127.67 (d, $J = 10.1$ Hz), 40.48 (s). UV–Vis (methanol) (nm (logε)): 330.4 (3.50), 267.4 (4.31), 209.6 (4.92).

$[RuH(NCO)(CO)(PPh_3)_2(NO_2PhCH_2py)]$ (2)

Yields 54 %. $C_{50}H_{41}N_3O_4P_2Ru$. Anal. calc. C 65.9 H 4.5 N 4.6 %. Anal. found. C 65.6 H 4.6 N 4.6 %. IR: 3,056 $\nu_{(ArH)}$; 2,234 $\nu_{(N=C\ from\ NCO)}$; 1,992, 1,971 $\nu_{(Ru–H)}$; 1,928 $\nu_{(CO)}$; 1,597 $\nu_{(asym\ NO2)}$; 1,479 $\delta_{(C–CH\ out\ of\ the\ plane)}$; 1,433 $\nu_{Ph(P–Ph)}$; 1,347 $\nu_{(sym\ NO2)}$; 1,330 $\nu_{(CO\ from\ NCO)}$; 1,090 $\delta_{(C–CH\ in\ the\ plane)}$; 741 $\delta_{(C–C\ out\ of\ the\ plane)}$; 693 $\delta_{(C–C\ in\ the\ plane)}$; 602 $\delta_{(NCO)}$; 518 $\nu_{(N;P–Ru)}$. ^{1}H NMR (400 MHz, $CDCl_3$) δ 8.34–8.17 (m, pybenzylNO$_2$), 7.62–7.50 (m, pybenzylNO$_2$), 7.39–7.09 (m, pybenzylNO$_2$, PPh$_3$), 7.07–6.97 (m, pybenzylNO$_2$), 3.85 (s, CH_2 from pybeznylNO$_2$), -7.11 (dt, $J = 103.6$, 24.5 Hz, $H_{(Ru)}$). ^{31}P NMR (202 MHz, $CDCl_3$) δ 45.49 (s, PPh_3). ^{13}C NMR (101 MHz, $CDCl_3$) δ 207.04 (s), 152.67 (s), 134.17 (d, $J = 5.6$ Hz), 133.85 (d, $J = 6.9$ Hz), 129.70 (s), 129.32 (d, $J = 9.9$ Hz), 128.98 (s), 127.79 (dt, $J = 12.5$, 4.7 Hz), 123.95 (d, $J = 5.3$ Hz), 40.48 (s). UV–Vis (methanol) (nm (logε)): 337.0 (4.26), 275.8 (4.86), 252.4 (5.02), 226.8 (5.27), 207.6 (5.62).

$[RuH(NCS)(CO)(PPh_3)_2(NO_2PhCH_2py)]$ (3)

Yield 63 %. $C_{50}H_{41}N_3O_3P_2RuS$. Anal. calc. C 64.8 H 4.5 N 4.5 %. Anal. found. C 64.6 H 4.5 N 4.5 %. IR: 3,055 $\nu_{(ArH)}$; 2,094 $\nu_{(N=C\ from\ NCS)}$; 2,006 $\nu_{(Ru–H)}$; 1,925 $\nu_{(CO)}$; 1,597 $\nu_{(asym\ NO2)}$; 1,479 $\delta_{(C–CH\ out\ of\ the\ plane)}$; 1,432 $\nu_{Ph(P–Ph)}$; 1,347 $\nu_{(sym\ NO2)}$; 1,090 $\delta_{(C–CH\ in\ the\ plane)}$; 742 $\delta_{(C–C\ out\ of\ the\ plane)}$; 694 $\delta_{(C–C\ in\ the\ plane)}$; 518 $\nu_{(N;P–Ru)}$. ^{1}H NMR (400 MHz, $CDCl_3$) δ 8.29–8.20 (m, pybenzylNO$_2$), 7.59–7.47 (m, pybenzylNO$_2$), 7.38–7.10 (m, PPh$_3$, pybenzylNO$_2$), 7.05 (dd, $J = 11.4$, 4.1 Hz, pybenzylNO$_2$), 6.96 (t, $J = 8.6$ Hz, pybenzylNO2), 3.87 (s, CH_2 from pybenzylNO$_2$), -7.18 (dt, $J = 100.0$, 24.4 Hz, $H_{(Ru)}$). ^{31}P NMR (162 MHz, $CDCl_3$) δ 39.42 (d, $J = 15.5$ Hz, PPh_3). ^{13}C NMR (101 MHz, $CDCl_3$) δ 206.92 (s), 152.72 (s), 134.77 (d, $J = 22.4$ Hz), 134.12 (t, $J = 5.9$ Hz), 133.95–133.66 (m), 133.42 (d, $J = 7.5$ Hz), 129.72 (s), 129.49 (d, $J = 6.5$ Hz), 129.14 (s), 128.54–127.41 (m), 124.28 (s), 123.98 (s), 40.50 (s). UV–Vis (methanol) (nm (logε)): 327.5 (4.43), 278.0 (4.81), 208.0 (5.68).

Physical measurements

Infrared spectra were recorded on a Nicolet iS5 FTIR spectrophotometer in the range 4,000–400 cm^{-1} using KBr pellets. Electronic spectra were measured on a Jasco V630 UV–VIS spectrophotometer in the range of 600–180 nm in methanol solutions. The ^{1}H, ^{31}P and ^{13}C NMR spectra were obtained at room temperature in $CDCl_3$ using a Bruker 500 MHz spectrometer. The ^{13}C NMR spectra was prepared as proton decoupled $^{13}C\{^{1}H\}$ spectra. Elemental analyses (C, H, N) were obtained on a Perkin–Elmer CHN–2400 analyzer. Powder X-ray diffraction (PXRD) measurements were performed on a PANalytical Empyrean X-ray diffractometer using Cu–Kα radiation ($\lambda = 1.5418$ Å), in which the X-ray tube was operated at 40 kV and 30 mA ranging from 5° to 80° (Supplementary Materials. Figure S1). The steady-state and time-resolved emission spectra were measured for EtOH:MeOH (4:1) solutions with a FLS-980 spectrophotometer at ambient temperature using a 450-W Xe arc lamp as a light source and PMT + 500 nm (Hamamatsu, R928P) in cooled housing as a detector. The Raman scattering of the solvent was always subtracted from the steady-state emission spectra of the complexes. The quantum yields of fluorescence were determined by absolute methods at room temperature, using the integrating sphere with solvent as a blank. The solutions of samples were first filtered and diluted to absorbance under 0.1 to avoid inner filter effects and the influence of impurities from the medium, then excited at the wavelength corresponding to the excitation maximum of the complexes. The time-resolved measurements were made in optically diluted ($0.05 < O.D < 0.1$) methanol: ethanol solutions at room temperature using time correlated single photon counting (TCSPC) methods on an FLS-980 spectrophotometer. The excitation wavelength (310 nm) was obtained using a picosecond pulsed diode EPLED-310 nm with 100 ns pulse period as light source. A PMT + 500 nm (Hamamatsu, R928P) in cooled housing was used as detector. The system was aligned at the emission wavelengths. Additionally, for the analysis of fluorescence decay, an instrument response function (IRF) needs to be obtained. The IRF contains information about the time response of the overall optical and electronic system. The IRF was designated using ludox solution as a standard at 310 nm. The influence of Raman scattering of the solvent on emission of the sample was avoided using a filter.

Computational methods

The calculations were carried out using the Gaussian09 [21] program. Molecular geometries of the singlet ground states of the complexes were fully optimized in the gas phase at the B3LYP level of theory [22, 23]. For each of the complexes, a frequency calculation was carried out, verifying that the optimized molecular structure corresponds to an energy minimum; thus, only positive frequencies were found. The DZVP basis set [24] with *f* functions with exponents 1.94722036 and 0.748930908 was used to describe the ruthenium atom, and the basis set used for the lighter atoms (C, N, O, S, P, H) was 6-31G with a set of d and p polarization functions (6-31G(2d,p) for sulfur, 6-31G** for carbon, nitrogen, and 6-31G(d,p) for hydrogen). The TD-DFT method [25] was employed to calculate the electronic absorption spectra of the complexes using the solvent Polarizable Continuum Model (PCM). The contributions of various atom groups (ligands, metal center) to each molecular orbital were calculated using Mulliken population analysis. GaussSum 2.2 [26] was used to calculate group contributions to the molecular orbitals and to prepare the density of states (DOS) diagrams. The DOS diagrams were created by convoluting the molecular orbital information with Gaussian curves of unit height and FWHM (Full Width at Half Maximum) of 0.3 eV.

Crystal structure determination and refinement

Crystals of the complexes (**1**)–(**3**) were mounted in turn on a Gemini A Ultra Oxford Diffraction automatic diffractometer equipped with a CCD detector for data collection. X-ray intensity data were collected with graphite monochromated MoK_α radiation ($\lambda = 0.71073$ Å) at a temperature of 295(2) K, with ω scan mode. Ewald sphere reflections were collected up to $2\theta = 50.10°$. Details concerning crystal data and refinement are gathered in Table 1. Lorentz, polarization and empirical absorption corrections using spherical harmonics implemented in the SCALE3 ABSPACK scaling algorithm [27] were applied. The structures were solved by the Patterson's method and subsequently completed by difference Fourier recycling. All the nonhydrogen atoms were refined anisotropically using full-matrix, least-squares techniques. All hydrogen atoms except H(Ru) were positioned in geometrically idealized positions and were allowed to ride on their parent atoms with Uiso(H) = 1.2 *Ueq*. The Ru–H hydrogen atoms were found from difference Fourier synthesis after four cycles of anisotropic refinement and refined as "riding" on the adjacent atom with an individual isotropic temperature factor equal to 1.2 times the value of the equivalent temperature factor of the parent atom, with geometry idealization after each cycle. Bearing in mind the limits of Fourier synthesis and the problems in recognizing artifacts in the immediate neighborhood of heavy atoms, it is doubtful if a reliable position for the hydrogen atom bound to the Ru atom can be found in the difference Fourier map whilst avoiding the danger of mistaking the effects of the

Table 1 Crystal data and structure refinement details of [RuHCl(CO)(NO_2PhCH_2py)(PPh_3)$_2$] (**1**), [RuH(NCO)(CO)(NO_2PhCH_2py)(PPh_3)$_2$] (**2**) and [RuH(NCS)(CO)(NO_2PhCH_2py)(PPh_3)$_2$] (**3**)

	1	2	3
Empirical formula	$C_{49}H_{41}ClN_2O_3P_2Ru$	$C_{50}H_{41}N_3O_4P_2Ru$	$C_{50}H_{41}N_3O_3P_2RuS$
Formula weight	904.30	910.87	926.93
Temperature (K)	295.0(2) K	295.0(2) K	295.0(2) K
Crystal system	Monoclinic	Monoclinic	Triclinic
Space group	$P2_1/c$	$P2_1/c$	P-1
Unit cell dimensions			
a (Å)	9.6791(4)	10.1700(5)	9.8744(14)
b (Å)	38.6997(13)	22.5135(8)	9.9679(9)
c (Å)	35.4623(16)	19.6361(14)	23.4817(19)
α (°)	90	90	99.318(7)
β (°)	96.626(5)	104.934(6)	101.484(9)
γ (°)	90	90	90.555(9)
Volume (Å^3)	13194.7(9)	4344.1(4)	2233.0(4)
Z	12	4	2
Calculated density (Mg/m^3)	1.366	1.393	1.379
Absorption coefficient (mm^{-1})	0.533	0.483	0.515
F(000)	5568	1872	952
Crystal dimensions (mm)	0.27 × 0.15 × 0.08	0.17 × 0.11 × 0.05	0.46 × 0.08 × 0.05
θ Range for data collection (°)	3.29–25.05	3.35–25.05	3.45–25.05
Index ranges	$-11 \le h \le 11$	$-12 \le h \le 10$	$-11 \le h \le 11$
	$-46 \le k \le 38$	$-21 \le k \le 26$	$-11 \le k \le 11$
	$-42 \le l \le 42$	$-16 \le l \le 23$	$-27 \le l \le 27$
Reflections collected	57,882	18,391	20,738
Independent reflections	23,344 [$R_{(int)} = 0.0886$]	7,664 [$R_{(int)} = 0.0589$]	7,894 [$R_{(int)} = 0.0393$]
Data/restraints/parameters	23,344/0/1579	7,664/0/545	7,894/0/545
Goodness-of-fit on F^2	0.959	0.959	1.041
Final R indices [$I > 2\sigma(I)$]	$R_1 = 0.0698$	$R_1 = 0.0552$	$R_1 = 0.0436$
	w$R_2 = 0.1251$	w$R_2 = 0.1116$	w$R_2 = 0.0967$
R indices (all data)	$R_1 = 0.1478$	$R_1 = 0.1037$	$R_1 = 0.0606$
	w$R_2 = 0.1544$	w$R_2 = 0.1283$	w$R_2 = 0.1039$
Largest diff. Peak and hole	0.955 and −0.454	0.877 and −0.454	0.485 and −0.272

series termination errors for a true atomic position. In the complexes, the Ru–H bond lengths, ranging from 1.52(6) to 1.92(4) Å, are acceptable. The OLEX2 [28] and SHELXS, SHELXL, SHELXH [29] programs were used for all the calculations. Atomic scattering factors were those incorporated in the computer programs.

The refinement of structure of (**1**) was difficult due to the large amount of atoms in the unit cell. The detected error resulted from distortion of a phenyl ring in PPh_3 has no bearing on the bond lengths and angles around the metal center. On the other hand, the crystals used for measurements were very well formed and the X-ray measurements taken several times for different monocrystals gave the same parameters. Similarly, after the addition of distance restraints to the C–C bonds (AFIX 66), the R values were not significantly improved.

Results and discussion

In the reaction between [RuHCl(CO)(PPh_3)$_3$] and 4-(4-nitrobenzyl)pyridine (NO_2PhCH_2py), the chloride hydride carbonyl complex with formula [RuHCl(CO)(PPh_3)$_2$ (NO_2PhCH_2py)] was obtained. The addition of stoichiometric amounts of cyanate or thiocyanate to the reaction mixture caused the removal of chloride from the coordination sphere and formation of complexes (**2**) and (**3**), respectively.

The ^{1}H NMR spectra of the complexes present expected signals from the aromatic rings of PPh_3 and 4-(4-nitrobenzyl)pyridine ligands. Moreover, the CH_2 moiety from the benzyl group gave a singlet near to 4.00 ppm. The signals at high field indicate the presence of the hydride ligands and were observed as a triplet (**1**) at −13.50 ppm and doublet of triplets (**2**, **3**) at −7.11 and −7.18 ppm, respectively. The differences in the shifts of these signals are due to differences between chloride and pseudohalide acceptor–donor properties. The ^{31}P NMR spectra of the complexes (**1**) and (**3**) (unlike complex (**2**), which showed a singlet) both show doublets suggesting distortion from the ideal *trans* disposition of triphenylphosphine ligands. However, distortions from ideal octahedral geometries in each of these complexes are comparable (P(1)–Ru(1)–P(2) angles); thus, this situation can result from coupling to the hydride ligand. Additionally, in the case of complex (**2**), the observed π–π stacking interactions between PPh_3 phenyl centroids and pyridine ring of the ligand are stronger than in the other two complexes, which may explain the presence of a singlet on the ^{31}P spectrum. In the ^{13}C NMR spectra of the complexes, sets of signals coming from the pyridine and phenyl rings are visible in regions of 150–145 and 130–123 ppm. A signal near to 40 ppm results from the presence of a –CH_2– carbon in the ligand structure. The pseudohalide ligands in complexes (**2**) and (**3**) are indicated by strong $\nu_{N=C}$ stretching bands at 2,234 and 2,094 cm^{-1}, respectively. For interpreting the vibrational spectra of complexes with ambidentate ligands such as thiocyanate, the wavenumber of $\nu_{C=N}$ is one of the factors that indicate the coordination mode. The complexes with N-bonded isothiocyanate ligands generally display the C=N stretching band in a lower region (around 2,050 cm^{-1}) than those with S–bonded thiocyanate (above 2,100 cm^{-1}). Hence, complex (**3**) substantially fulfills this criterion. However, the frequency of this band is also sensitive to the co-ligands. Thus, in the determination of the coordination mode of thiocyanate ligands, X-ray analysis is essential in most cases. The hydride and carbonyl ligands gave bands for ν_{Ru-H} and ν_{CO} at 2,017, 1,919 cm^{-1} for (**1**), 1,971, 1,928 cm^{-1} for (**2**) and 2,006, 1,925 cm^{-1} for (**3**). In the vibrational spectrum of the parent [RuHCl(CO)(PPh_3)$_3$] complex, the ν_{Ru-H} and ν_{CO} are visible at 2,020 and 1,922 cm^{-1}, respectively. In the case of complexes (**2**) and (**3**), the influences of the coordinated pyridine rings are clearly visible in the decreasing frequencies of the Ru–H stretching bands. The nitro group from 4-(4-nitrobenzyl)pyridine gave asymmetric stretching bands at 1,594, 1,597 cm^{-1} and symmetric stretches at 1,347, 1,343 cm^{-1}.

Molecular structures

Crystals of the complexes (**1**)–(**3**) suitable for single-crystal X-ray analyses were obtained by slow evaporation of the reaction mixtures. The crystals of complexes (**1**) and (**2**)

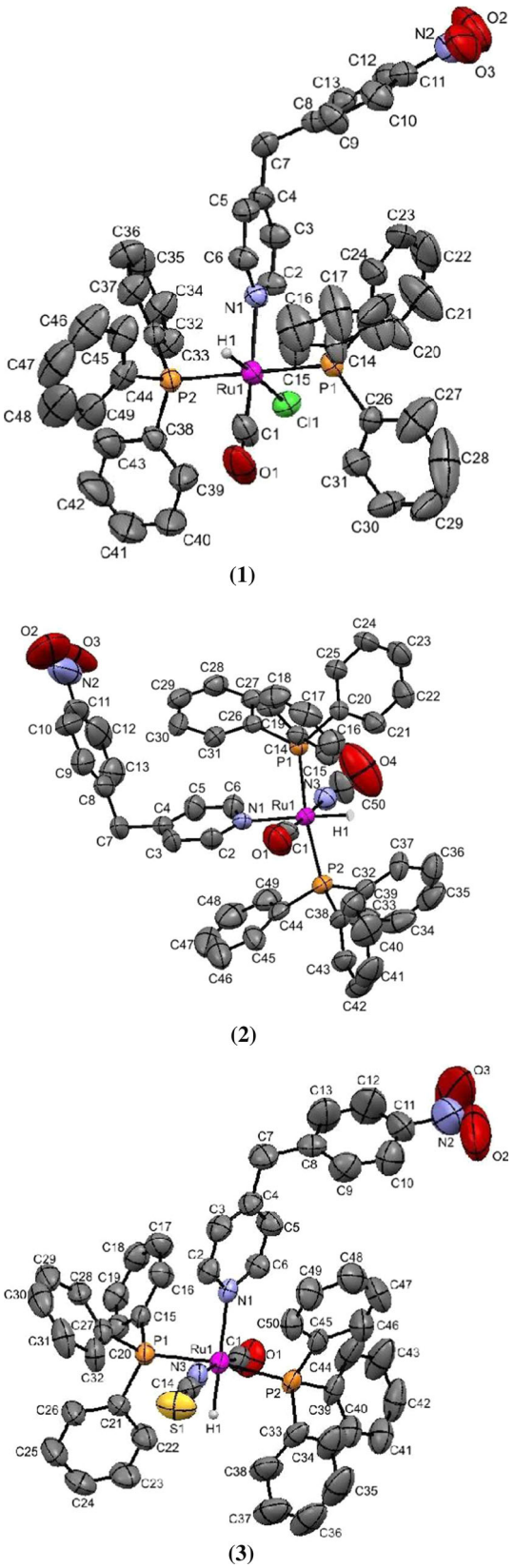

Fig. 1 Molecular structure of the (**1**), (**2**) and (**3**) complexes with 30 % probability displacement ellipsoids. Hydrogen atoms (except Ru–H) are omitted for clarity

Table 2 Selected experimental bond lengths (Å) and angles (°) for [[RuHCl(CO)(NO_2PhCH_2py)(PPh_3)$_2$] (**1**), [RuH(NCO)(CO)(NO_2PhCH_2-py)(PPh_3)$_2$] (**2**) and [RuH(NCS)(CO)(NO_2PhCH_2py)(PPh_3)$_2$] (**3**)

	(**1**)			(**2**)	(**3**)
(Å)	Ru(1)	Ru(2)	Ru(3)		
Ru(1)–C(1)	1.790(8)	1.823(8) [1.86]	1.811(7)	1.843(5) [1.86]	1.823(3) [1.87]
Ru(1)–N(1)	2.209(5)	2.180(4) [2.27]	2.185(4)	2.232(4) [2.34]	2.229(3) [2.34]
Ru(1)–N(3)				2.057(5) [2.13]	2.094(3) [2.12]
Ru(1)–P(1)	2.3553(16)	2.3567(17) [2.43]	2.3446(16)	2.3515(12) [2.43]	2.3622(8) [2.45]
Ru(1)–P(2)	2.3438(16)	2.3505(16) [2.44]	2.3461(19)	2.3478(13) [2.42]	2.3565(9) [2.43]
Ru(1)–H(1)	1.92(4)	1.827(18) [1.61]	1.52(6)	1.64(3) [1.61]	1.59(3) [1.60]
Ru(1)–Cl(1)	2.5206(16)	2.5256(16) [2.59]	2.5305(16)		
C(1)–O(1)	1.158(8)	1.140(8) [1.16]	1.145(7)	1.178(6) [1.17]	1.138(4) [1.16]
(°)					
C(1)–Ru(1)–N(1)	170.1(3)	170.8(3) [171.18]	169.2(2)	90.9(2) [92.51]	97.82(12) [96.30]
C(1)–Ru(1)–N(3)				177.9(2) [178.32]	172.88(13) [175.74]
C(1)–Ru(1)–P(1)	89.2(2)	88.8(2) [88.14]	90.2(2)	89.91(16) [95.14]	87.80(11) [91.84]
C(1)–Ru(1)–P(2)	89.9(2)	90.8(2) [88.96]	88.0(2)	93.15(16) [90.18]	92.11(11) [92.82]
N(1)–Ru(1)–P(1)	89.44(13)	89.27(13) [90.98]	89.13(14)	94.01(10) [94.67]	94.92(6) [93.19]
N(1)–Ru(1)–P(2)	91.03(13)	90.87(12) [91.64]	91.01(13)	93.06(10) [94.12]	92.43(6) [95.00]
N(3)–Ru(1)–P(1)				88.53(12) [84.12]	93.07(7) [88.07]
N(3)–Ru(1)–P(2)				88.57(12) [90.79]	86.12(7) [86.64]
P(1)–Ru(1)–P(2)	177.41(6)	178.08(6) [176.69]	171.32(6)	172.25(5) [169.51]	172.59(3) [170.08]
C(1)–Ru(1)–Cl(1)	99.8(3)	99.6(3) [101.16]	101.7(2)		
N(1)–Ru(1)–Cl(1)	90.02(14)	89.54(13) [87.65]	88.95(13)		
N(1)–Ru(1)–N(3)				87.87(16) [86.05]	89.15(10) [87.96]
P(1)–Ru(1)–Cl(1)	91.12(6)	93.00(6) [93.20]	97.05(6)		
P(2)–Ru(1)–Cl(1)	91.43(6)	88.92(5) [88.94]	91.62(6)		
C(1)–Ru(1)–H(1)	78.7(14)	84.4(12) [86.43]	85(2)	89.5(9) [90.06]	85.6(10) [86.35]
N(1)–Ru(1)–H(1)	91.5(13)	86.7(12) [84.76]	85(2)	178.0(9) [177.39]	176.2(10) [177.27]
N(3)–Ru(1)–H(1)				91.8(9) [91.38]	87.4(10) [89.40]
P(1)–Ru(1)–H(1)	90.7(13)	91.4(13) [87.97]	89(2)	88.0(9) [85.54]	87.0(10) [87.40]
P(2)–Ru(1)–H(1)	86.7(13)	86.7(12) [90.25]	82(3)	84.9(9) [85.41]	85.6(10) [84.17]
Cl(1)–Ru(1)–H(1)	177.6(12)	174.2(11) [172.34]	174(2)		
Ru(1)–C(1)–O(1)	174.5(8)	174.8(8) [176.22]	174.8(6)	175.3(5) [178.20]	176.7(3) [178.80]
Ru(1)–N(3)–C(50)				168.5(5) [160.72]	170.5(3) [175.51]

Calculated values are given in square brackets

belong to the monoclinic $P2_1/c$ space group, whilst complex (**3**) crystallizes in the triclinic *P*-1 space group. In the structure of complex (**1**), three independent molecules exist in the asymmetric units. Figure 1 displays an *ORTEP* representation of one molecule of complex (**1**) and the molecular structures of (**2**) and (**3**); selected experimental bond distances and angles are collected in Table 2. The coordination environments around the ruthenium(II) centers in the complexes have distorted octahedral geometry, defined by two axial phosphorus donors from triphenylphoshine, plus hydride, carbonyl, halide and NO_2PhCH_2py ligands in the equatorial plane. The bond distances and angles in the complexes are in good agreement with the reported data for similar complexes [30–33]. The angles between the two PPh_3 ligands range from 175.6° in (**1**, average value) to 172.25(5)° in complex (**2**).

The main structural differences between these complexes are visible in the equatorial plane; in the chloride complex (**1**), a carbonyl ligand occupies the *trans* position relative to the NO_2PhCH_2py ligand, while in the isocyanate and isothiocyanate complexes (**2**) and (**3**), the carbonyl is *trans* to the pseudohalide ligand. The carbonyl C(1)–O(1) distance in complex (**3**) is shorter than those in (**1**) and (**2**), due to the enhanced Ru(II) → NCS backbonding via the involvement of the σ-donating and π-accepting carbonyl ligand *trans* to NCS^-.

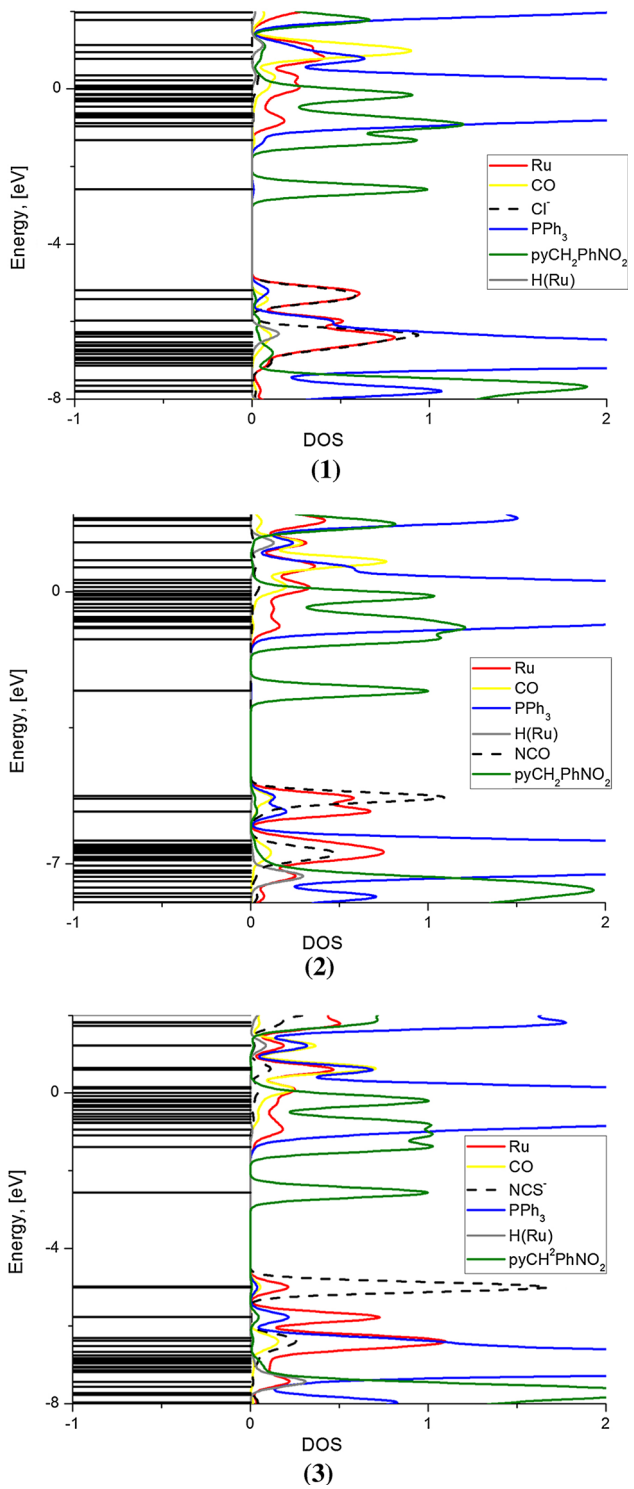

Fig. 2 DOS diagrams of complexes (**1**)–(**3**)

The structures of the complexes show intra- and intermolecular short contacts (Supplementary Materials, Table S1) which, according to Desiraju and Steiner, can be classified as weak hydrogen bonds [34]. Graph set analysis show that the hydrogen bonds do not create any additional structures. Moreover, analysis of the molecular arrangements in the crystal structures of these complexes indicates some electronic interactions between the pyridine and phosphine phenyl rings. Taking into account the mutual geometries of the rings (Supplementary Materials, Table S2), these can be considered as intramolecular π···π interactions.

Quantum calculation

The ground state geometries of the complexes were optimized in the singlet state, using the B3LYP functional. The calculations were carried out for the gas phase molecules, and in general, the calculated geometries are in agreement with the experimental data (see Table 2). The calculations on complex (**1**) were performed for the geometry of molecule Ru(2). The calculated bond lengths and angles are overestimated by about 0.1 Å and 5°, which can be explained by the neglect of intermolecular interactions for the gas phase.

Based on the optimized geometries of the complexes, NBO analyses were performed in order to reveal the nature of the coordination between ruthenium and the donor atoms of the ligands. These analyses showed that the bonding between the 4-(4-nitrobenzyl)pyridine and ruthenium is largely noncovalent; the Coulomb-type interaction between the ruthenium center and 4-(4-nitrobenzyl)pyridine ligand is clearly visible in the calculated Wiberg bond indices, which are considerably lower than one, being equal to 0.3831 (**1**), 0.3418 (**2**) and 0.3422 (**3**). The Ru–P bond orders are also smaller than 1 (0.7). The Wiberg indexes of the CO bonds in the complexes are reduced (by about 0.2) with respect to free CO ($W_{CO} = 2.23$). The maximum reduction of Wiberg index is calculated for complex (**2**), which is consistent with the lowest charge on the carbonyl ligand (0.171), while for complexes (**1**) and (**3**), the calculated natural charges on the carbonyl ligands are increased to 0.211 and 0.200, respectively. However, the natural charges on ruthenium are lowest in complex (**1**) (−0.911), whilst in the pseudohalide complexes, due to different configuration of equatorial plane, the values are close to −0.84. The donations from the ligands to the metal have the advantage over the back donations from the metal to ligands, especially in the presence of strong π-acceptor carbonyl ligands; thus, the calculated natural charges are considerably lower than +2.

Analysis of the frontier molecular orbitals is useful for understanding the spectroscopic properties such as electronic absorption and emission spectra. The partial density of state diagrams, presented in Fig. 2, shows a substantial share of d_{Ru} and chloride or pseudohalide orbitals in the HOMO. In complex (**1**), *d*-ruthenium and chloride contribute the 49 and 42 %, respectively, to the HOMO. In pseudohalide complexes (**2**) and (**3**), the

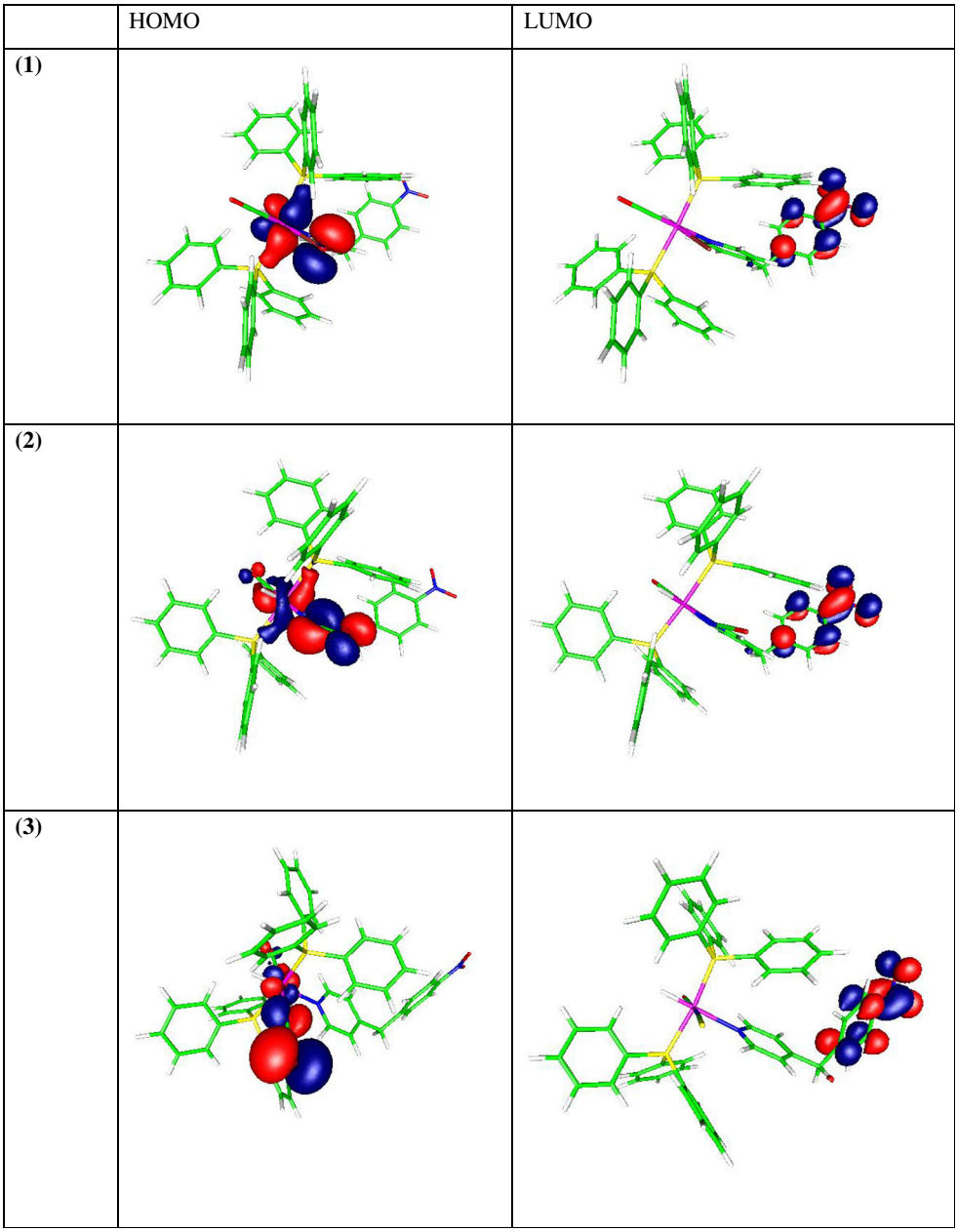

Fig. 3 Contours of HOMO and LUMO in (**1**), (**2**) and (**3**) complexes

share of ruthenium decreases to 26 and 13 %, while the participation of NCO^- and NCS^- increases to 58 and 82 %, respectively. Moreover, in the HOMO's of the chloride and isocyanate complexes, as distinct from complex (**3**), the triphenylphosphine ligands take part (about 10 %). The ruthenium *d* orbitals play substantial role, up to 73 % for the isothiocyanate complex, in the MO's ranging from HOMO-1 to HOMO-3. The LUMOs of the complexes are localized on π^* orbitals of 4-(4-nitrobenzyl)pyridine, and for this reason, there are no significant differences in the energies of the LUMO in these complexes. The contours of the HOMO and LUMO of the complexes are presented in Fig. 3.

Electronic absorption and emission spectra

Experimental electronic absorption spectra of the complexes are presented in Fig. 4. There are two bands in the range 330–250 nm and a high energy band with maximum near 210 nm resulting from transitions in the PPh_3 ligands and/or from $\pi \rightarrow \pi^*$ excitations in the NO_2PhCH_2py ligand. This is also typical of other recently characterized hydride carbonyl ruthenium(II) complexes with pyridine-type ligands [18, 32]. In the low energy region, weak bands above 300 nm were calculated transitions in which the HOMO, HOMO-1/-3 and LUMO, LUMO + 1, LUMO + 2 are engaged, and in accordance with the

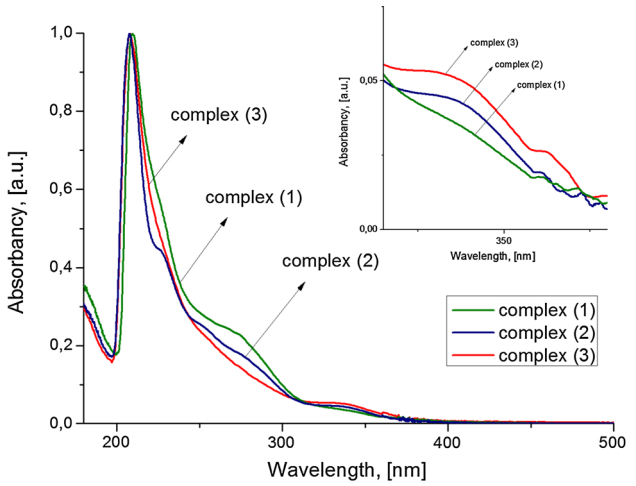

Fig. 4 Experimental absorption spectra of the (**1**)–(**3**) complexes. Inset graph: absorption band corresponding to the excitation wavelength

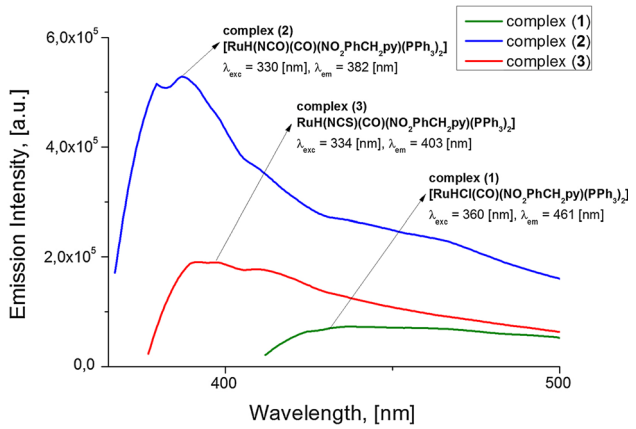

Fig. 5 Emission spectra of (**1**), (**2**) and (**3**) complexes

determined electronic structures of the complexes, the bands have Metal to Ligand Charge Transfer (MLCT) character with admixture of Ligand to Ligand Charge Transfer (LLCT). The bands in the vicinity of 250 nm can be described as LLCT transitions with small amount of MLCT character.

Under the same conditions as used for the complexes, the free NO_2PhCH_2py ligand is nonemissive in excitation wavelengths between 250 and 500 nm (Supplementary Material, Figure S2). Moreover, the free ligand has recently been characterized as nonluminescent [35]. The solutions of the complexes excited at 360, 330 and 334 nm exhibit weak emission maxima at 461, 382 and 403 nm, for complexes (**1**), (**2**) and (**3**), respectively. The photoluminescence (PL) spectra are shown in Fig. 5. The shift of the excitation and emission maxima to lower energy in the case of (**1**) may be connected with the comparatively higher participation of ruthenium in the occupied frontier orbitals. On the other hand, the determined Stokes shifts are equal to 4,578.92 cm^{-1} (**1**), 4,125.02 cm^{-1} (**2**) and 5,126.22 cm^{-1} (**3**) and this parameter usually decreases with an increase of LLCT character in the excited state. Moreover, from the emission spectra, it can be seen that the PL intensity is the highest in the case of isocyanate complex (**2**); the quantum Φ_{em} is 0.17 %. Complexes (**1**) and (**3**) show quantum yields under 0.01 %; thus, we can conclude that they are practically nonluminescent. Careful inspection of the calculated transitions close to the excitation energies shows substantial share of LLCT in the case of complex (**2**), which explains the value of the Stokes shift as well as the relatively high quantum yield. For complexes (**1**) and (**3**), however, the calculated transitions show increasing share of d-ruthenium orbitals (50 and 64 %, respectively); hence, the excited state can be characterized as MLCT admixture with LLCT. In Table 3, the selected calculated transitions and orbital compositions are presented. The photoluminescence lifetime measurements were made at room temperature using the time correlated single photon counting (TCSPC) method with excitation at 310 nm to eliminate solvent scattering. In each case, bi- or tri-exponential decay models were used to quantitatively fit the measured curves (Supplementary Materials, Figure S3). The longest lifetime was measured for the strongest emissive isocyanate complex (**2**) (see Table 4). The low quantum yields and short lifetimes for these complexes probably result from an easily obtained crossing point between the charge transfer state and MC state. This was confirmed by the calculation on the triplet state (spin density map), which indicated the localization of spin density on the ruthenium atom (Supplementary Materials, Figure S4).

Conclusions

A series of $[RuHX(CO)(pyCHPhNO_2)(PPh_3)_2]$ complexes, where X = Cl, NCO, or NCS and $pyCHPhNO_2$ = 4-(4-nitrobenzyl)pyridine, were obtained and structurally and spectroscopically characterized. The free pyridine derivative is known to be nonemissive, but its complexes reveal weak photoluminescence. The character of the excitation bands depends mostly on the character of the HOMOs, which are partially localized on *d*-ruthenium orbitals and chloride/pseudohalide ligands. Thus, the excitation transitions can be identified as having MLCT character with admixture of LLCT. The determined Stokes shifts, quan-

Table 3 Selected calculated transitions and correspond orbitals compositions

Complex	Energy (nm)	Transition	Orbital composition (L = pyCHPhNO$_2$)
(1)	375.4	H-2 → LUMO (99 %)	Ru(50 %) + PPh_3(42 %) → L(99 %)
	360.2	HOMO → L+2 (69 %)	Ru(49 %) + Cl(42 %) + PPh_3(9 %) → PPh_3(19 %) + L(80 %)
(2)	338.6	H-3 → LUMO (95 %)	Ru(23 %) + PPh_3(73 %) → L(100 %)
	324.2	H-4 → LUMO (56 %)	PPh_3(92 %) → L(100 %)
(3)	337.5	H-3 → LUMO (98 %)	Ru(64 %) + CO(11 %) + NCS(19 %) → L(100 %)
	324.1	HOMO → L+2 (65 %)	Ru(13 %) + NCS(82 %) → L(100 %)

Table 4 Spectroscopic properties of the complexes

Complex	λ^A_{EX} (nm)	λ^A_{EM} (nm)	Φ^B_{EM}	τ^C_{EM} (ns)	$E_G^{OPT,\ d}$ (eV)	$E_G^{CALC,\ e}$ (eV)	E^E_{HOMO} (eV)	E^E_{LUMO} (eV)
(1)	360	461	<0.0001	6.9	2.88	3.11	−5.68	−2.58
(2)	330	382	0.0017	7.5	3.25	3.08	−5.65	−2.57
(3)	334	403	<0.0001	4.8	3.08	3.22	−5.77	−2.56

[a] Determined at 298 K in MeOH:EtOH (1:4)

[b] Absolute quantum yields measured in MeOH:EtOH (1:4) mixture at room temperature

[c] Obtained by TSCPS method in optically diluted solutions (OD < 0.1) at 298 K in MeOH:EtOH (1:4) with excitation wavelength 340 nm. Average values obtained from bi- or tri-exponential fitting measured curves

[d] Estimated from emission maximum $E_g^{opt} = 1{,}241/\lambda_{em}$

[e] Calculated at B3LYP/DZVP level

tum yields and lifetimes show that isocyanate complex has the strongest emissive nature, which is connected with substantial LLCT character of the fluorescence. However, the chloride and isothiocyanate complexes are practically nonemissive, with quantum yields under 0.01 %. The values of the lifetimes and low quantum yields are the characteristics of ruthenium(II) complexes, in which easily obtained ^{3}MC states impact on emissive MLCT/LLCT states.

Supplementary Data

CCDC 978367, 978365 and 978366 contain the supplementary crystallographic data for the complexes (**1**), (**2**) and (**3**), respectively. These data can be obtained free of charge via http://www.ccdc.cam.ac.uk/conts/retrieving.html or from the Cambridge Crystallographic Data Centre, 12 Union Road, Cambridge CB2 1EZ, UK; fax: +44 1223-336-033; or e-mail: deposit@ccdc.cam.ac.uk.

Acknowledgments The GAUSSIAN-09 calculations were carried out in the Wrocław Centre for Networking and Supercomputing, WCSS, Wrocław, Poland, http://www.wcss.wroc.pl.

References

1. Wagenknecht PS, Ford PC (2011) Coord Chem Rev 255:591
2. Yersin H, Rausch AF, Czerwieniec R, Hofbeck T, Fischer T (2011) Coord Chem Rev 255:2622
3. Oner I, Sahin C, Varlikli C (2012) Dyes Pigm 95:23
4. Fantacci S, De Angelis F (2011) Coord Chem Rev 255:2704
5. Yin J-F, Velayudham M, Bhattacharya D, Lin H-C, Lu K-L (2012) Coord Chem Rev 256:3008
6. Takahashi Y, Arakawa H, Sugihara H, Hara K, Islam A, Katoh R, Tachibana Y, Yanagida M (2000) Inorg Chim Acta 310:169
7. Dosioa F, Stella B, Ferrero A, Garinob C, Zonari D, Arpicco S, Cattel L, Giordanoa S, Gobetto R (2013) Int J Pharm 440:221
8. Iizuka N, Motoki S, Nakai M, Nakabayashi Y (2014) Inorg Chem Commun 46:145
9. Huanga S, Zhu F, Qiua H, Xiao Q, Zhou Q, Su W, Hu B (2014) Colloids Surf, B 117:240
10. Ma J, Wu J, Liu W, Wang P, Fan Z (2012) Spectrochimica Acta Part A 94:340
11. Slim M, Sleiman HF (2004) Bioconjugate Chem. 15:949
12. Shan B-Z, Zhao Q, Goswami N, Eichhorn DM, Rillema DP (2001) Coord Chem Rev 211:117
13. Bomben PG, Robson KCD, Koivisto BD, Berlinguette CP (2012) Coord Chem Rev 256:1438
14. Tyson DS, Luman CR, Zhou X, Castellano FN (2001) Inorg Chem 40:4063
15. Pradhan B, Das S (2008) Chem Mater 20:1209
16. Wang P, Humphry-Baker R, Moser JE, Zakeeruddin SM, Grätzel M (2004) Chem Mater 16:3246
17. Stufkens DJ, Vlček A Jr (1998) Coord Chem Rev 177:127
18. Małecki JG, Krompiec S, Maroń A, Penkala M (2012) Polyhedron 48:21

19. Małecki JG, Maroń A, Gryca I, Mori A, Suzuki T (2013) Polyhedron 62:188
20. Ahmad N, Levinson JJ, Robinson SD, Uttely MF (1974) Inorg Synth 15:48
21. Gaussian 09, Revision A.1, M. J. Frisch, G. W. Trucks, H. B. Schlegel, G. E. Scuseria, M. A. Robb, J. R. Cheeseman, G. Scalmani, V. Barone, B. Mennucci, G. A. Petersson, H. Nakatsuji, M. Caricato, X. Li, H. P. Hratchian, A. F. Izmaylov, J. Bloino, G. Zheng, J. L. Sonnenberg, M. Hada, M. Ehara, K. Toyota, R. Fukuda, J. Hasegawa, M. Ishida, T. Nakajima, Y. Honda, O. Kitao, H. Nakai, T. Vreven, J. A. Montgomery, Jr., J. E. Peralta, F. Ogliaro, M. Bearpark, J. J. Heyd, E. Brothers, K. N. Kudin, V. N. Staroverov, R. Kobayashi, J. Normand, K. Raghavachari, A. Rendell, J. C. Burant, S. S. Iyengar, J. Tomasi, M. Cossi, N. Rega, J. M. Millam, M. Klene, J. E. Knox, J. B. Cross, V. Bakken, C. Adamo, J. Jaramillo, R. Gomperts, R. E. Stratmann, O. Yazyev, A. J. Austin, R. Cammi, C. Pomelli, J. W. Ochterski, R. L. Martin, K. Morokuma, V. G. Zakrzewski, G. A. Voth, P. Salvador, J. J. Dannenberg, S. Dapprich, A. D. Daniels, O. Farkas, J. B. Foresman, J. V. Ortiz, J. Cioslowski, D. J. Fox (2009) Gaussian, Inc., Wallingford CT
22. Becke AD (1993) J Chem Phys 98:5648
23. Lee C, Yang W, Parr RG (1988) Phys. Rev. B 37:785
24. Eichkorn K, Weigend F, Treutler O, Ahlrichs R (1997) Theor Chim Acc 97:119
25. Casida ME (1996) In: Seminario JM (ed) Recent developments and applications of modern density functional theory, theoretical and computational chemistry, vol 4. Elsevier, Amsterdam, p 391
26. O'Boyle NM, Tenderholt AL, Langner KM (2008) J Comp Chem 29:839
27. CrysAlis RED, Oxford Diffraction Ltd., Version 1.171.29.2
28. Dolomanov OV, Bourhis LJ, Gildea RJ, Howard JAK, Puschmann H (2009) J Appl Cryst 42:339
29. Sheldrick GM (2008) Acta Cryst. A 64:112
30. Małecki JG, Maroń A (2013) Transition Met Chem 38:133
31. Małecki JG, Maroń A (2013) Polyhedron 55:18
32. Małecki JG, Maroń A (2012) Transition Met Chem 37:727
33. Małecki JG, Maroń A (2012) Transition Met Chem 38:419
34. Desiraju GR, Steiner T (1999) The weak hydrogen bond in structural chemistry and biology. IUCr Monograph on Crystallography 9. Oxford University Press, Oxford
35. Chan C-W, Lai T-F, Che C-M, Peng S-M (1993) J Am Chem Soc 115:11245